Available online at www.sciencedirect.com

ScienceDirect

Ceramics International 40 (2014) 1675–1686

CERAMICS INTERNATIONAL

www.elsevier.com/locate/ceramint

Foaming performance of aqueous albumin and mullite-albumin systems used in cellular ceramic processing

M.L. Sandoval*, M.A. Camerucci

División Cerámicos, INTEMA (UNMdP–CONICET), Av. J. B. Justo 4302 (7600), Mar del Plata, Argentina

Received 10 May 2013; received in revised form 10 July 2013; accepted 11 July 2013
Available online 20 July 2013

Abstract

Bovine serum albumin (BSA) solutions (5, 10 and 15 vol%) and stabilized aqueous mullite (40 vol%)–BSA (5, 10 and 15 vol%) suspensions were foamed by mechanical stirring at 2300 rpm. The colloidal and rheological behaviors of suspensions were studied by measuring zeta potential and shear flow properties, respectively. The foaming performance of aqueous systems was evaluated by characterizing the foaming capacity and the foam stability by volume and electrical conductivity measurements. Overrun % was considered as a measure of the foaming capacity, while the variation of this parameter, the foam wetness (Φ_{FW}) and the foam density stability (*FDS %*) with the stand time and the time to half collapse ($t_{1/2}$) were evaluated in order to study the stability of foamed systems. Median bubble diameters, bubble size distribution widths and bubble shape factors as a function of time were determined by analyzing images captured by confocal laser-scanning microscopy (CLSM). The results related to the stability of foamed systems were used to evaluate the global destabilization mechanism of these systems, analyzing, in particular, the influence of the solid particles in the protein foam. The obtained results are useful for studying the shaping of cellular mullite green bodies from the thermogelation of foamed aqueous ceramic-protein suspensions.

Keywords: A. Suspensions; D. Mullite; Foams; Foaming capacity; Foam stability

1. Introduction

Ceramic foams are a type of porous materials with high porosity. They are cellular structures formed by a three-dimensional solid network whose more relevant specific properties, such as low density, low thermal conductivity, high surface area, and high permeability determine their technological fields of application (filtration, thermal or acoustic insulating, catalysis, impact-absorbing structures, pre-forms for metal–ceramic composites, biomedical implants, scaffolds for cell growth and high efficiency combustion burners, among others) [1,2]. Cell size, morphology, and degree of interconnectedness are also relevant factors that help determine potential applications for these materials [3]. In particular, closed-cell materials are needed for thermal applications, while open-cell materials are required for uses such as filters and catalysts. Besides the microstructural features and properties of these materials, which are specially given by the presence of the cells, the ceramic matrix composition must also be selected properly [1–4]. Mullite ceramics ($2SiO_2 \cdot 3Al_2O_3$) in particular are important materials due to their good mechanical properties at high temperature as well as their low thermal conductivity, low thermal expansion coefficient and good chemical stability. These properties are the reasons why highly porous mullite materials are amply used. Recently, a renewed interest in these materials has arisen due to the new requirements for materials that are being used in emerging technologies (i.e. development of metal–mullite composites and porous mullite materials used in the filtration and emission control of fine particles in the automobile industry) [5–7].

A variety of processing routes is needed in order to make cellular materials since different properties are required to cover different applications; no route is sufficiently flexible to yield all the necessary structures [3]. The selection of a specific processing route depends on the required microstructure, as

*Corresponding author. Tel.: +54 223 4816600; fax: +54 223 4810046.
E-mail address: laura.sandoval@fi.mdp.edu.ar (M.L. Sandoval).

0272-8842/$ - see front matter © 2013 Elsevier Ltd and Techna Group S.r.l. All rights reserved.
http://dx.doi.org/10.1016/j.ceramint.2013.07.059

well as on inherent aspects of the process such as cost, simplicity, environmental impact and versatility. The main processing methods for these materials can be divided into three categories, each one including some variations: the replication technique, the direct-foaming technique and the sacrificial template method [4].

In recent years, one of the most promising processing methods has been the direct consolidation method, in which a ceramic suspension consolidates inside non-porous molds through the formation of a physical or chemical gel on cooling or on heating, without compaction or removal of solvent. Among them, an innovative non-contaminant colloidal processing is based on thermal consolidation (at temperatures lower than 90 °C) by gelling an aqueous ceramic suspension foamed with globular proteins (i.e. albumin) and the formation of a macro-cellular ceramic structure after removing organics at high temperature [1,4,8–11]. This processing method thus combines the direct-foaming technique with on-site forming by thermo-gelling a ceramic-protein suspension. Therefore, a globular protein, an environmental-friendly agent, acts as both a foaming and binder/consolidator agent of the ceramic suspension. These properties are associated with the ability of globular proteins to act as a surfactant reducing the surface tension of gas–liquid interfaces and thus stabilize the gas bubbles developed within the suspension (the proteins adsorb at the air–water interface and their structure unfolds, which increase the hydrophobicity of the film favoring the foaming), and form a gel in water after heating to 70–80 °C. The gel formation is related to the denaturation of the proteins, the subsequent formation of aggregates and their cross-linking in order to generate a three-dimensional polymeric network. After burn-out and sintering treatments, a macro-cellular ceramic structure is produced in which the number of cells and their sizes depend on foamed suspension properties and the ability of protein molecules to stabilize foam before gelling process occurs (the gas bubbles have to remain occluded into the ceramic suspension a certain time). When the films surrounding these bubbles remain intact until consolidation, a closed-cell foam is formed, while open-cell foams are produced when the films are partially broken [3]. In this context, the evaluation of properties of the wet foams is key because they mainly determine the characteristics of the cellular microstructure. Many factors related to protein or other components in the mixture influence the foam properties; such as protein solubility and concentration, ionic strength, pH, concentration, type and form of addition of the processing additives and the presence of ceramic particles. Moreover, the stability and the viscoelastic properties of the wet foams depend on bubble size distribution and bubble morphology.

Numerous papers about protein foams, in particular those based on albumin, have been published because these systems play an important role in both food and biotechnological processes [12–15]. However, a few papers related to the processing of ceramic materials have been reported, although the behavior and properties of ceramic-protein wet foams rarely were evaluated [9–10,16,17]. In this context, both the quality and the stability of wet foams are critical aspects that should be studied because they determine, in part, the characteristics and homogeneity of the developed cellular microstructure.

In this paper, the foaming performance of mullite-albumin suspensions was evaluated by characterizing their foaming capacity and foam stability. The results obtained are useful in order to study the shaping of cellular mullite green bodies from the thermogelation of foamed aqueous ceramic-protein suspensions.

2. Experimental procedure

2.1. Raw materials

A high-purity commercial mullite ($3Al_2O_3 \cdot 2SiO_2$) powder (MULS, Baikowski, France) was used as the ceramic raw material. The impurity level determined by wet chemical analysis was less than 0.2 wt%. The weight percentages of the elements (expressed in oxides) were also determined from this analysis. An excess of alumina (even considering that all the silica calculated is part of the mullite) with respect to the stoichiometric composition (Al_2O_3=71.8 wt%, SiO_2=28.2 wt %) was determined. This result is in agreement with the crystalline phases identified by X-ray diffraction analysis (XRD) (X'Pert PRO, PANalytical, radiation of CuK_α at 40 mA and 40 kV, and at 1°2θ/min), which are mullite as primary phase (File 74-2419), and α-alumina (File 82-1399), θ-alumina (File 11-0517) and cristobalite (File 77-1317) as secondary phases. In addition, a low intensity band located in the zone of the more intense diffraction peaks corresponding to the silica polymorphs (20–30 °2θ), which is associated with non-crystalline silicate phases, was observed. The powder density value measured by He-pycnometry (Multipycnometer, Quantachrome Co., USA) was 3.07 g/cm^3. This value was lower than the theoretical densities of the mullite (3.16 g/cm^3) and α-Al_2O_3 (3.98 g/cm^3) due to the contribution of the crystalline θ-alumina (3.28 g/cm^3) and cristobalite (2.30 g/cm^3) phases and the non-crystalline silicate phases (~2.2 g/cm^3), which have lower densities. On the other hand, the mullite powder presented a medium crystallinity that was associated, in part, with the presence of little narrow and medium height diffraction peaks compared to the characteristic peaks of diffractograms of the highly crystalline commercial mullite powders [18]. Based on these results, it can be inferred that the commercial mullite powder come from a synthesis in which the total conversion of the starting mixture (ammonium alum and silica) was not achieved [19]. The powder presented a bimodal particle size distribution (Mastersizer S, Malvern Instruments Ltd., UK) with a low mean volume diameter (D_{50} = 1.46 μm), a high volume percentage (~30%) of fine particles < 1 μm, and agglomerates up to 50 μm which were associated with the presence of the very fine particles. These results together with the powder characteristics and the identified phases are consistent with the high value of specific surface area (13.5 m^2/g) determined by the BET method (Monosorb, Quantachrome Co., USA). The field emission scanning electron microscopy (FESEM, Hitachi S-4700, Japan) micrograph of the mullite powder is shown in Fig. 1.

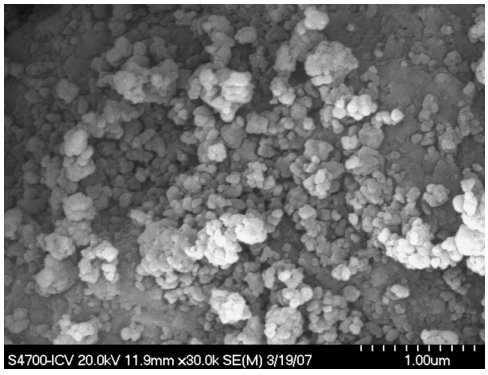

Fig. 1. FE-SEM micrograph of commercial mullite powder.

Very small three-dimensional particles, some of them faceted, with equiaxial morphology, constitute the mullite powder. Agglomerates of the smallest particles can also be observed, which is in agreement with the granulometric analysis.

A commercially available bovine serum albumin (BSA; A7906, Sigma-Aldrich) of high purity (> 98%), with a density of 1.27 g/cm^3 measured by He-pycnometry (Multipycnometer, Quantachrome Co., USA), 583 amino-acids, a molecular weight of 66.5 kDa [20] and an isoelectric point (IEP) around 4.8–5.2 [21,22] was employed as a foaming agent and consolidator/binder agent of the ceramic suspension.

2.2. Preparation and characterization of aqueous albumin and mullite-albumin systems

Stable aqueous mullite suspensions (40 vol%; pH=8.7) with 5, 10 and 15 vol% of BSA were prepared by mixing (impeller mixer with flat blades) mullite and BSA powders (dissolved previously in water) with 0.45 wt% of commercial ammonium polyacrylate solution (Dolapix CE-64, Zschimmer & Schwarz, Germany) as a dispersant, and by homogenization in a ball mill for 4 h (alumina rods of 9 mm diameter and 9 mm length were used as milling media in a milling media/mullite ratio of 0.75) to stabilize the suspension. In addition, aqueous BSA solutions of 5, 10 and 15 vol% with a phosphate buffer were prepared by stirring BSA powder in water and 0.45 wt% of Dolapix CE-64 with respect to the solid content for 10 min. Thus, BSA solutions were prepared in experimental conditions (pH, type and concentration of dispersant) similar to the aqueous systems with mullite particles (i.e. mullite-BSA suspensions).

The optimum stability conditions for preparing the aqueous mullite suspensions were determined by measuring zeta potential (Zetasizer Nano ZS, Malvern Instruments, UK) and shear flow properties (Haake RS50, Thermo electron Corp., Germany), which were reported in a previous paper [23]. In this paper, the stability of aqueous mullite-BSA suspensions was also determined by measuring zeta potential (Zetasizer Nano ZS, Malvern Instruments, Germany) and shear flow properties. The zeta potential measurements were carried out by employing solutions highly diluted (0.01 wt%) with 0.45 wt % of Dolapix CE-64 as a dispersant and by adding KCl solution (10^{-2} M) as an inert electrolyte in order to keep the ionic force of the solution constant. The pH was adjusted by hydrochloric acid HCl (10^{-1} M). From these tests, isoelectric points (IEP) of aqueous mullite-BSA suspensions were determined and compared with the mullite one, which was determined in the same experimental conditions. Viscosity measurements at room temperature were performed employing a rotational rheometer (MCR 301 Anton-Paar Physics, Germany) under controlled-rate operating modes with a coaxial cylinder sensor (gap, 1 mm). A three-stage measuring program with a linear increase of shear rate from 0 to 1000 s^{-1} in 300 s, 60 s at 1000 s^{-1}, and further decreasing to zero shear rate in 300 s was used.

2.3. Foaming of aqueous albumin and mullite-albumin systems

BSA and mullite-BSA wet foams were produced by stirring at 2300 rpm for 10 min in a graduated acrylic cylindrical container 76 mm in diameter and 120 mm in height using an turbine-style impeller mixer with four asymmetric concave blades of 10 mm in length, 5 mm in width and 1 mm thick. The blade type was designed from a commercial device and previously selected from experimental tests (Fig. 2). The stirring rate was previously selected from foam initial volume ('foaming capacity') measurements (Overrun %, Eq. (4)) using BSA solutions foamed with the selected impeller mixer at 1700, 2300 and 3400 rpm during 10 min. For every BSA concentration, the foams generated at 1700 rpm showed the lowest foam capacities (~140%) while those obtained at 3400 rpm presented the highest values (250%), with the foam capacities obtained at 2300 rpm (210%) in the middle. However, at the highest rate (3400 rpm), the precipitation of aggregates was observed, which was attributed to the denaturation of the protein molecules (two-state transition phenomenon for which the protein is unfolded) due to the fact that they were subjected at a high mechanical shear [21].

Based on these tests and considering that the foaming capacity obtained at 2300 rpm is adequate in order to prepare foam ceramic, this rate was chosen as a foaming rate. Four acrylic blades 6 mm in width and 120 mm in height were placed inside of the container in order to act as deflector plates. These deflector plates deviate the turbulent flow during high-rate mixing and minimize the formation of a vortex generated

Fig. 2. Image of the turbine-style impeller mixer with four asymmetric concave blades used to create foam.

by the centrifugal force acting over the liquid, which enhances the efficiency of mixing. The impeller was selected taking into account that the impeller type, among others factors, determines the foam volume as much as the quality of the generated foam. Asymmetric concave blades disperses the gas into the liquid more efficiently than the simple flat blades because the former distribute the gas throughout the entire liquid volume from bottom to top, providing better mass transfer and uniformity throughout the container′s volume. The container′s geometrical dimensions were established in order to achieve optimum mixing and foaming from the following relations [24]:

$$0.33 \leq \left(\frac{B_d}{D}\right) \times n_d \leq 0.5 \quad (1)$$

$$d_i \approx \frac{D}{3} \quad (2)$$

$$0.15 \leq \left(\frac{b_i}{D}\right) \times n_d \leq 0.30 \quad (3)$$

where D is the diameter of the container, B_d is the width of deflector plates, n_d is the number of deflector plates, d_i is the diameter of the impeller and b_i is the width of impeller blades.

2.4. Evaluation of foamed aqueous albumin and mullite-albumin systems

Foaming properties were characterized by the initial foam volume or foaming capacity (i.e. capacity of the continuous phase to include air or another gas) and the foam volume decrease by increasing time or foam stability (i.e. the foam′s ability to retain the gas for a certain period of time). There are several methods for measuring these properties. One of the most common (called volumetric method) consists of measuring the height of the foam and liquid by direct readings in a graduated container (± 0.5 mm) as a function of time in order to calculate, with the corresponding volumes, the parameter called Overrun %. However, in the case of ceramic systems, the foam and liquid heights cannot be easily visualized due to the presence of the solid particles suspended in the liquid phase, which hide the bubbles. So, in these systems, the foam volume decrease and the rate of fluid leakage from foam as a function of time cannot be accurately determined by the volumetric method. On the other hand, it should be also taken into account that although the volume of foam apparently remains fixed, the thickness of foam film, the bubble size and the amount of adsorbed fluid changes gradually with time [25]. Since foams generated from ceramic suspensions consist of a number of bubbles separated by liquid and solids films, foaming properties can be estimated by measuring their electric conductivities. The adsorbed water surrounding the bubbles is the main conductor medium. Electric conductivity measurements have been used by some authors to determine the liquid amount occluded into foams [25–28]. It has been reported that this method is more accurate in measuring the liquid trapped within foam than the volumetric method [27]. In this paper, the foaming capacity and foam stability of both systems were also determined by measuring their electric conductivity. Tests were performed using a conductivity meter (GW Instek SFG-1013; Digital Multimeter Rigol DM3062) and an electrode of stainless steel parallel plates 12.5×12.5 mm^2 and 0.3 mm thick with a separation distance of 25.5 mm. An AC carrier effective voltage of 1.0 V was applied across the electrode at a frequency of 25 kHz. The electrode was introduced 15.0 mm below the foam surface located in the graduated container. This kind of electrode minimizes the perturbation of the foamed system while maintaining uniform electrical fields between its surfaces. The shape and size, separation distance, relative position in the container and excited frequency of the electrical current, all which determine the current density between electrodes, were carefully chosen because these factors affect the accuracy of experimental data [27].

Based on the above, for BSA and mullite-BSA foams, the value of the Overrun % (relative error ~10%) at zero time, determined by measuring the volume, was considered to evaluate the foaming capacity. Many authors use this parameter in order to characterize the amount of air incorporated into the liquid phase, but there is no widespread agreement on the way to calculate it [29]. In this paper, the following equation was considered:

$$\text{Overrun}\% = 100 \times \left(\frac{V_T - V_L}{V_L}\right) \quad (4)$$

where V_T is the total volume (foam volume plus liquid volume) and V_L is the initial liquid volume [30,31].

In addition, variations of this parameter and foam wetness, Φ_{FW} defined as the ratio between the amount of liquid inside the foam and the foam volume plus the liquid volume inside the foam, with stand time, t_S (0, 10, 15, 20 and 30 min) were evaluated in order to study the foam stability. The foam wetness was calculated using the following equation:

$$\Phi_{FW} = \frac{(V_L - V_{Lne})}{(V_T - V_{Lne})} \quad (5)$$

where V_{Lne} is the volume of liquid that is not trapped inside the foam [32].

Regarding the conductimetric technique, the electric conductivity of the foam (C_i) measured immediately after producing each foamed system and foam electric conductivity as a function of stand time, t_S (C_t) were used to characterize the foam density stability (*FDS* %), which was calculated from Eq. (6), and time to half collapse, $t_{1/2}$ (time for which the foam density stability decreased by 50%) [12].

$$FDS(\%) = \frac{C_t}{C_i} \times 100 \quad (6)$$

On the other hand, Φ_{FW} can also be calculated as a function of time from the following equation [33]:

$$\frac{C_t}{C_s} = \frac{2\phi_{FW}}{3 - \phi_{FW}} \quad (7)$$

In general, the parameters calculated from conductivity measurements showed a relative error of $< 10\%$. Bubble size distributions of foamed BSA solutions and foamed BSA-mullite suspensions as a function of stand times (0, 10 and 30 min) were obtained by analyzing images captured by confocal laser-scanning microscopy, CLSM (Nikon C1, Japan). This technique enables high quality images of the foams generated from ceramic-protein systems to be obtained, which is difficult to achieve by optical microscopy. The light source was an argon ion laser with a $\lambda = 512$ nm. Rhodamine B (tetraethyl rhodamine) 0.1 wt% was used as a water-soluble fluorescent dye that binds to protein molecules without interfering with ceramic particles. Thus, the aqueous protein solution is shown as the lighter phase while air bubbles are black. Images were corrected by regulating brightness and contrast. Number-weighted bubble size distributions were obtained directly from the analysis of the corresponding images by using image analysis software (Image-Pro Plus 7.0, Media Cybernetics). The characteristic parameters, such as median bubble diameters, D_{50} and distribution width (this parameter was taken as $W = D_{90} - D_{10}/D_{50}$ where D_{90} and D_{10} are the bubble diameters for 90 and 10% of bubbles, respectively) were determined by analyzing between 100 and 200 objects. The average value of the circularity of bubbles ($4\pi A/p^2$) was also determined from measurements of the area (A) and perimeter (p) of each object.

The results obtained by evaluating the physical and morphological parameters that characterize the foamed systems as a function of stand time were used in order to determine the destabilization mechanism of the generated wet foams in the studied time range. Finally, the influence of the ceramic particles in the stability of the foams was also analyzed.

3. Results and discussion

3.1. Aqueous mullite and mullite-BSA suspensions

3.1.1. Colloidal stability

The zeta potential (ξ) vs. pH curves of mullite-BSA suspensions are shown in Fig. 3. In this figure, the results corresponding to the aqueous mullite suspension were also included for comparative purposes. From these curves, the isoelectric point values (IEP) for studied systems were determined. For the aqueous mullite suspension, a value of IEP = 7.0 was obtained, while the IEP values were ~5.0 for all the mullite-BSA suspensions. The isoelectric point of the mullite suspension decreased by adding protein. This result indicates that a specific adsorption of the protein on the mullite particle surface occurred, and consequently, the particle surface charge was changed [22,34]. The shift in the pH value, which is a function of the adsorbed protein mass, reached the saturation value at pH ~5 since this value corresponds to the IEP of the protein. According to the IEP (5.0), at the pH value (8.7) employed in the preparation of the suspensions, the protein is negatively charged and determines, together with the used organic dispersant (polyelectrolyte), a potential zeta value ($\xi = -34$ mV) for all the mullite-BSA suspensions higher than

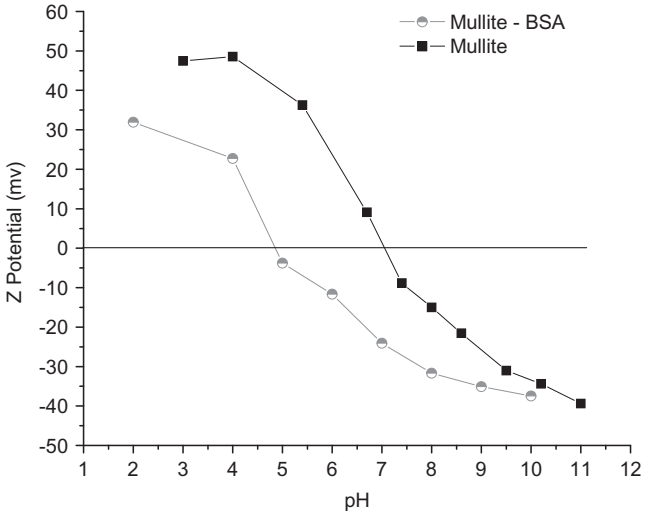

Fig. 3. Curves of zeta potential (ξ) vs. pH of aqueous mullite suspension and mullite-BSA suspensions.

that obtained for the aqueous mullite suspension ($\xi = -23$ mV). Thus, an adequate colloidal stability of the ceramic-protein system was obtained at pH 8.7. This result indicates that the aqueous mullite suspension is stabilized through synergistic interaction of the protein and the polyelectrolyte (Dolapix CE-64) by an electrostatic and steric stabilization mechanism. From previous studies carried out with the mullite powder used in this work [35], it was inferred that not all adsorption sites are covered by the specific adsorption of the polyelectrolyte, leaving sites available for protein adsorption. The obtained results are in agreement with reported data regarding albumin adsorption on ceramic particles [34]. It has been determined that the more negative the zeta potential value of the ceramic material, the higher the absorption of albumin. The adsorption mechanism is believed to be a multistep process, where the proteins can be found in many different conformational states induced by electrostatic interaction. It is worth noting that the protein undergoes hardly any conformational changes in the range of pH employed [22]. Rezwan et al. [22] reported that one side-on monolayer of BSA (theoretically, a BSA amount of 230 ng/cm^2 is required) is required to completely change the surface charge of ceramic particle to the surface charge of BSA. They proposed a two-step adsorption model for BSA on alumina particles at pH 7, which involves the formation of one side-on monolayer and the additional adsorption of proteins forming dimers with those from the first monolayer. This adsorption occurs when the surface charge of the particle is completely masked and the IEP cannot shift further than the IEP of the protein (process based on protein/protein interaction). Taking into account these reports, the obtained results and the similar chemical and physical characteristics of the mullite particles with respect to the studied alumina powder, a two-step adsorption model for BSA on mullite particles could be assumed. On the other hand, the influence of others chemical (e.g. foreign groups chemically bonded with molecules on the surface, molecular arrangement on the surface) and physical (e.g. capillary

absorption, mechanical trapping on roughness) factors in the bond strength of the adsorbed protein molecules cannot be ruled out [34].

3.1.2. Shear flow properties

Shear stress and apparent viscosity curves as a function of shear rate at room temperature for the aqueous mullite and mullite-BSA (5, 10 and 15 vol%) suspensions are shown in Fig. 4a and b, respectively. Apparent and relative viscosity values of these suspensions are given in Table 1. The relative viscosity was defined as the ratio of the apparent viscosity of the mullite-BSA suspension and the apparent viscosity of the BSA-free mullite suspensions (all the suspensions with 40 vol % of total solid loading).

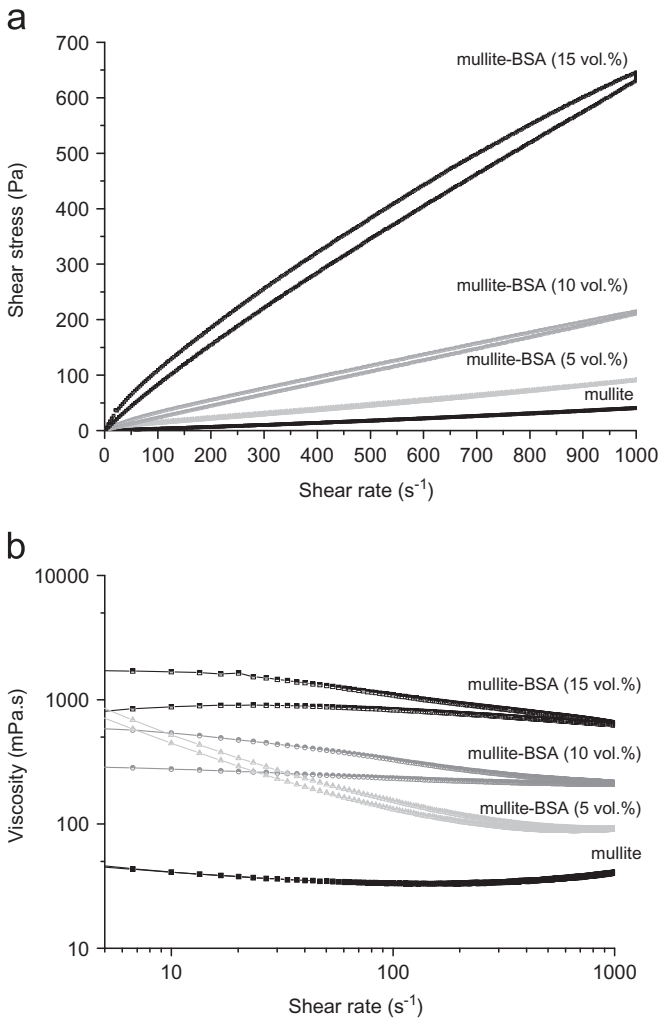

Fig. 4. Shear stress (a) and viscosity (b) curves as a function of aqueous mullite-BSA (0, 5, 10 and 15 vol%) suspensions at room temperature.

The aqueous mullite suspension showed a typical rheological behavior of a complex-fluid, exhibiting a slight transition from pseudoplastic to dilatant behavior for shear rates higher than 300 s^{-1} and a progressive decreasing of the viscosity while maintained for 60 s at the highest shear rate (1000 s^{-1}) as was reported in a previous work [23]. Moreover, the suspension presented a low thixotropic thickening (~170 Pa/s; measured as the area between the up and down curves), which can be associated with the high solid loading (40 vol%) and type of dispersant employed (polyelectrolyte). It is assumed that ceramic particles form a two dimensional structure for low shear rates and a disordered three dimensional structure for high shear rates. When the disordered structure is maintained at a constant shear rate for a certain time, particles are rearranged in a more stable two dimensional structure [36]. Additionally, the presence of albumin in the aqueous mullite suspension changed the global rheological behavior of the suspension. The apparent viscosity of the mullite suspension increased notably throughout the entire shear rate range by increasing the BSA content although this increment was much more marked at lowest shear rates (Table 1). Moreover, the dilatancy observed in the mullite suspension from ~300 s^{-1} was decreased and the thixotropic thickening was significantly increased as the albumin content increased (2500; 9200 and 31,300 Pa/s for mullite-BSA 5, 10 and 15 vol %, respectively). The aqueous mullite-BSA (15 vol%) suspension showed a clear pseudoplastic behavior (the suspension did not show dilatancy) highly time dependent. This behavior can be associated with the rearrangement of the ceramic particles in the flow direction and the extension of the protein chains preventing the formation of a three dimensional structure and allowing the formation of a new structure with a more stable configuration. Moreover, the dependency of the viscosity with time can be related to the presence of a large amount of protein also acting as a binder for the concentrated ceramic suspension.

3.2. Foamed aqueous BSA and mullite-BSA systems

3.2.1. Evaluation of foaming capacity and foam stability of BSA solutions

The spontaneous adsorption of globular proteins from solution to the air/water interface is the central factor that

Table 1
Apparent (η_{1000} and η_{10}) and relative (η_r) viscosity of aqueous mullite-BSA suspensions.

Systems	η_{10} (mPa s)	η_{1000} (mPa s)	η_r (at 10 s^{-1})	η_r (at 1000 s^{-1})
Mullite	41	40	1	1
Mullite-BSA (5 vol%)	521	91	13	2
Mullite-BSA (10 vol%)	538	215	13	5
Mullite-BSA (15 vol%)	1680	646	41	16

explains their performance as an agent foaming. This phenomenon is thermodynamically favorable due to the simultaneous dehydration of the hydrophobic interface and hydrophobic portions of the protein. The hydrophobic patches on the surface of the protein due to the hydrophobic amino acid residues drive this process, and then, once contacts with the interface are made, the natural flexibility within the molecules allow the previously buried hydrophobic portions to become exposed to the interface leading to interfacial denaturation of the molecules. Thus, during the adsorption process, the protein molecule undergoes a change in its conformation, an unfolding process in which hydrophobic regions of the protein molecule are reoriented toward the interface. Besides adsorption itself, others factors, such as heat and the addition of chemical agents, both of which increase the exposure of the hydrophobic regions, will increase protein surface activity [37]. In the case of BSA, it has been reported that the majority of damage occurs in the tertiary structure of the protein [38]. One of the main consequences of the protein adsorption at the air/water interface is its effectiveness at lowering the interfacial energy or the surface tension at the gas–liquid interface, which improves the foamability (e.g. the surface tension of the water is ~72 mN/m at room temperature, while the equilibrium surface tensions of the concentrated protein solutions are often around 45 mN/m) [14]. On the other hand, the electrostatic interactions also play a significant role in the protein adsorption process. It has been reported that the foaming properties of proteins are improved near their isoelectric points where the zeta potential is null. However, in the case of ceramic-protein systems, as studied in the present work, it is worth noting that the value of the zeta potential is determined by the interactions between the system components (ceramic particles–dispersant and ceramic particles–protein), and using a suspension prepared at pH value close to the IEP is not recommended since the system is not sufficiently stabilized in this condition (low value of zeta potential).

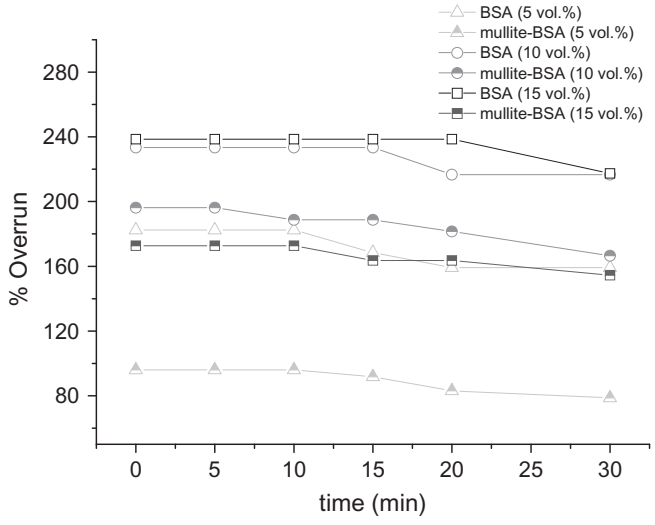

Fig. 5. Overrun % as a function of time for foamed BSA solutions and aqueous mullite-BSA suspensions.

In summary, when air is incorporated into an aqueous protein solution or into an aqueous ceramic suspension containing proteins, foam is formed, and it remains stable a certain amount of time due to protein adsorption at the bubble surface. Proteins functioning as foaming agents must have the ability to (a) adsorb rapidly at the air/water interface; (b) show rapid conformational change and rearrangement at the interface, and (c) form viscoelastic films via intermolecular interactions. The first two requirements are essential for foam generation, while the third is closely related to the stability of the foam.

The variation of the Overrun % (parameter determined from Eq. (4) to characterize the amount of air incorporated into the liquid phase) as a function of the stand time, t_S for aqueous BSA solutions and aqueous mullite-BSA suspensions prepared at 2300 rpm are shown in Fig. 5. Curves of foam wetness, ϕ_{FW} vs. stand time for aqueous BSA solutions determined from volumetric and electrical conductivity measurements and for aqueous mullite-BSA suspensions determined from electrical conductivity measurements are shown in Fig. 6a and b, respectively. The foaming capacity of the different BSA

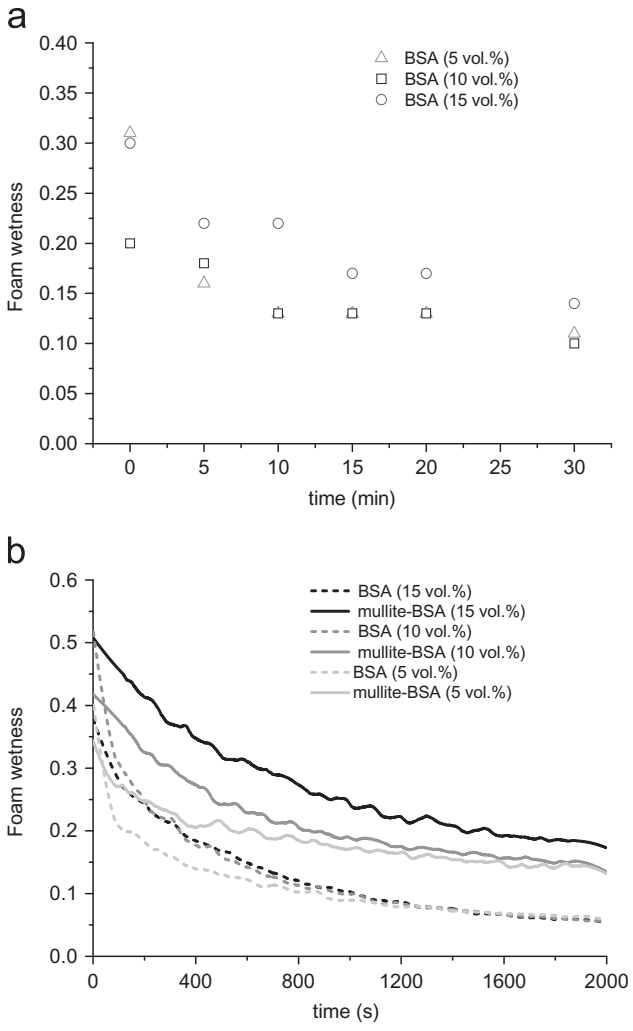

Fig. 6. Foam wetness (Φ_{FW}) as a function of time determined by volumetric (a) and conductimetric (b) methods.

solutions (5, 10 and 15 vol%) increased by increasing the BSA amount because a higher amount of air is incorporated and entrapped into liquid when the BSA amount increased (Fig. 5). This parameter was similar for 10 and 15 vol% of BSA indicating that a limit value was achieved for 2300 rpm. Initial foam wetness values (Φ_{FW} values at $t_S=0$) for all BSA concentrations determined by the volumetric method were between 0.20 ± 0.03 and 0.31 ± 0.04 (Fig. 6) and resulted slightly lower than those obtained from electrical conductivity measurements ($\Phi_{FW}=0.35 \pm 0.03$–0.50 ± 0.04). The obtained range of Φ_{FW} indicates that the generated foams were wet foams (dry foams have a Φ_{FW} much less than 0.01) [3,21].

Regarding the influence of the stand time, the trend of Overrun % values showed that in general they remained constant up to 10–15 min depending on BSA amount and then, with a further increase in time, the values decreased. The difference between the initial value of this parameter and the value achieved after 30 min decreased by increasing BSA content (19% for 5 vol% of BSA and 8.5% for 10 and 15 vol% of BSA). This parameter only takes into account the collapse of the foam due to the exposed film rupture, which can be considered as the final step in the global destabilization of the foam.

The Φ_{FW} values (Fig. 6) obtained by both methods decreased by increasing time until values between 0.06 and 0.15, depending on the method employed, were achieved; in other words, the foams remained wet even after 30 min (Φ_{FW} values determined by the conductimetric method were similar for the three BSA concentrations). It is worth noting that foam wetness fractions decreased significantly (in general greater than ~50% of its initial value) during the first 10 min, and then, with a further increase in the time, the diminution of Φ_{FW} values was much slower. In particular, the behavior of Φ_{FW} values determined by the conductimetric method indicates that for lowest BSA amount, Φ_{FW} decreased more quickly during the first 10 min than the others concentrations that showed similar behavior. Therefore, the analysis of the variation of foam wetness fraction with the stand time revealed, unlike the Overrun %, that a certain degree of foam destabilization associated mainly with drainage of liquid phase occurred from the first minutes after its generation. Also, *FDS %* values (parameter that characterizes the foam density stability which was calculated from Eq. (6)) for BSA foams (Fig. 7) strongly decreased for up to about 15 min, independently of the protein concentration as was already determined by Φ_{FW} variation with the stand time. However, the decrease rate of this parameter, which can be related to the drainage rate, was lower for the highest BSA concentration. In addition, the values of the time to half collapse ($t_{1/2}$) (Table 2) depended on the BSA concentration, with the order 15 vol% > 10 vol% > 5 vol%., which is in agreement with the fact that concentrated protein solutions give slightly more stable foams than dilute solutions. After 30 min, *FDS %* was less than 15% for all the BSA foams, indicating that practically all the bubbles had collapsed.

It is well known that the drainage involves physical separation between the gaseous and liquid phases of the foam due to gravity′s effect. In draining foams, light bubbles move upwards forming a denser foam layer on the top, while the heavier liquid phase is concentrated on the bottom. Foam drainage depends on the foam network geometry and properties related to liquid flow (e.g. density and viscosity). However, wet foams are thermodynamically unstable systems due to their gas–liquid interfacial area, and consequently, several physical processes besides drainage take place in them which decrease the overall system′s free energy and leads to their destabilization. Besides drainage (creaming), the main foam destabilization mechanisms include the independent but interrelated processes of coalescence of neighboring bubbles due to rupture of interbubble lamellae (film rupture) and join of two bubbles to generate a bigger bubble, and Ostwald ripening, which is a coarsening process caused by interbubble gas transport (disproportionation). The protein layer adsorbed onto the bubbles' surface imparts surface rigidity as well as electrostatic and steric repulsive interactions between bubbles which prevent coalescence. The more rigid the bubble surfaces, the lower the driven shear flow through channels. Moreover, slower drainage delays coarsening due to thicker film and less pressure gradients between bubbles. Thus, the drainage rate is controlled by the size of the Plateau borders as well as the rheological properties of the bulk liquid and gas/liquid interfaces. Contrary to dry foams, in wet foams drainage

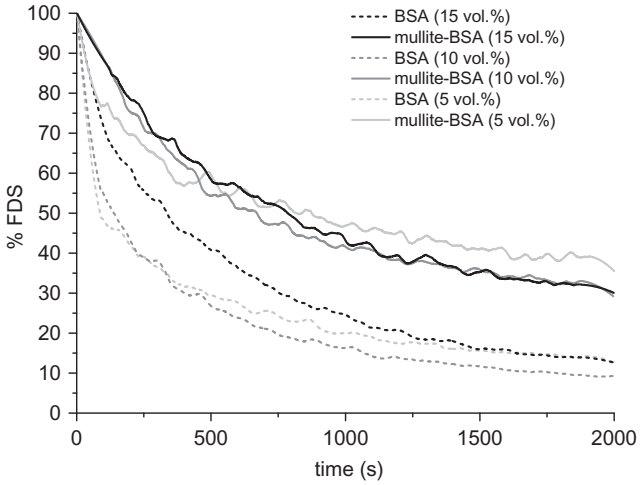

Fig. 7. Foam density stability (*FDS %*) as a function of time for foamed aqueous BSA solutions and mullite-BSA suspensions.

Table 2
Time to half collapse ($t_{1/2}$) values for foamed aqueous BSA solutions and mullite-BSA suspensions.

Systems	t_{50} (min)
BSA (5 vol%)	1.28
BSA (10 vol%)	2.20
BSA (15 vol%)	5.37
Mullite-BSA (5 vol%)	13.40
Mullite-BSA (10 vol%)	11.10
Mullite-BSA (15 vol%)	13.06

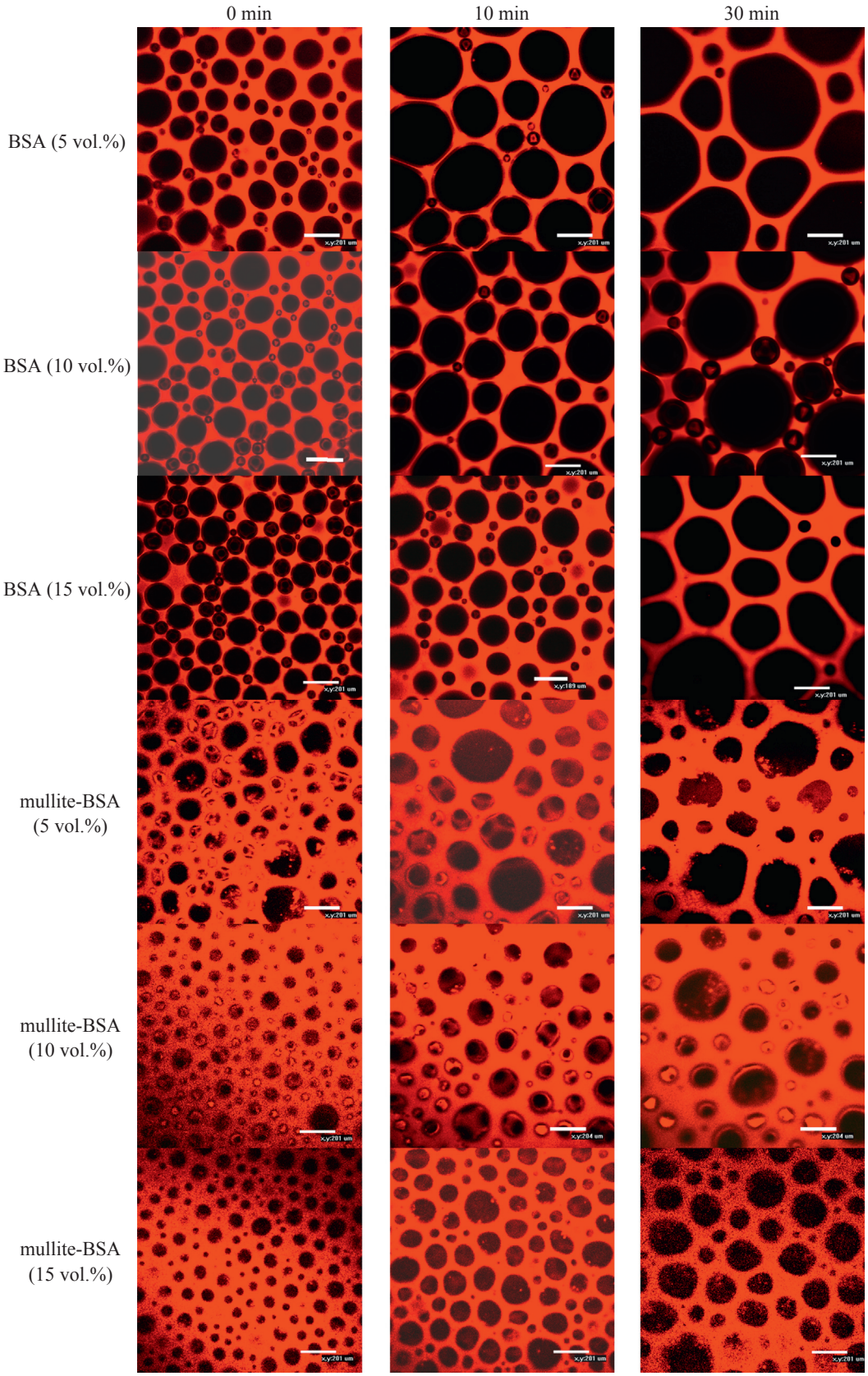

Fig. 8. Confocal laser-scanning microscopy images of BSA foams (5, 10 and 15 vol%) (a) and mullite-BSA (5, 10 and 15 vol%) foams (b) at $t_S = 0$, 10 and 30 min. (Bars = 200 μm).

Table 3
Bubble size distribution parameters as a function of stand time.

Systems	D_{50} (mm)			W		
	0 min	10 min	30 min	0 min	10 min	30 min
BSA (5 vol%)	0.12	0.15	0.18	1.1	1.8	3.9
BSA (10 vol%)	0.10	0.17	0.24	1.1	2.5	1.8
BSA (15 vol%)	0.17	0.19	0.19	1.2	1.9	2.0
Mullite-BSA (5 vol%)	0.10	0.10	0.13	1.1	1.7	1.6
Mullite-BSA (10 vol%)	0.06	0.09	0.11	1.3	1.5	1.5
Mullite-BSA (15 vol%)	0.05	0.10	0.14	1.3	1.3	1.4

occurs first as a result of the thick interstitial films, and only when these films become thinner do coalescence and coarsening occur.

Based on the above, the bubble size distributions as a function of the stand time must be considered alongside the evaluated parameters, in order to complete the analysis of the stability of foams and thus to establish their global destabilization mechanism. Confocal laser-scanning microscopy images of the foams captured as a function of stand time are shown in Fig. 8, and the characteristics parameters of bubble size distributions are given in Table 3. The features of these distributions are dictated by the interfacial properties and the thickness of the film between bubbles. Concurrence between the bubble expansion kinetics and the setting of the structure controls the foam cell size. For $t_S=0$, all the BSA foams presented the lowest mean bubble diameter (D_{50}) and width (W) of bubble size distributions. In general, for each stand time analyzed, except for 30 min, the D_{50} slightly increased and the width of the bubble size distributions remained approximately unchanged by increasing the BSA amount. In particular, for the highest time analyzed (30 min), the mean bubble diameter did not change by increasing the protein content. In addition, for all the BSA contents, D_{50} and W of the bubble size distributions increased by increasing the stand time. This behavior can be associated mainly with the occurrence of Ostwald ripening and coalescence due to the thinning of the bubble films. Ostwald ripening process involves gas transfers from small bubbles to large ones; therefore, big bubbles are growing while small bubbles are shrinking and bubbles of intermediate size either grow or shrink, which explains the increase of the bubble distribution width. In general, the registered changes were more marked between 0 to 10 min. However, for 15 vol% of BSA, the increase of the mean bubble size was less significant. This result could be associated with the assumption that in this foam the drainage of the liquid phase occurred more slowly and thus delayed the coarsening due to thicker lamellae between bubbles. This explanation could be also supported if it is taken into account that the viscosity of the protein solutions generally increase exponentially with protein concentration, which is attributable to increased interaction between the hydrated protein molecules.

On the other hand, the value of circularity (0.98 ± 0.02) of bubbles determined for all BSA foams at $t_S=0$ indicates that initially, the bubbles presented a high degree of sphericity, which agrees with the fact that every foam formed was wet (wet foams with high area of liquid–gas interface tend to adopt a spherical morphology). This morphologic parameter did not show any significant change by increasing time.

Based on the analysis of obtained results concerning BSA foams, it can be assumed that their destabilization occurred mainly by drainage during the first minutes of stand time and before 10 min, the destabilization can already be attributed to coalescence and Ostwald ripening events of bubbles affecting bubble size distribution (increase of D_{50} and W). However, the joint occurrence of these last processes with the drainage of the liquid phase cannot be ruled out. In protein foams, it is most likely that several of the destabilization mechanisms are occurring simultaneously [14].

3.2.2. *Influence of mullite particles on BSA foam properties*

Modifications that increase the foaming solution viscosity increase the foam stability by decreasing drainage rate [14]. However, the viscosity should not be so high as to strongly reduce the foaming capacity. Thus, the presence of ceramic particles in the protean aqueous system modified both aspects – the foaming capacity and the stability – of BSA foams. As expected, for all the BSA amounts, the foaming capacity of the protein in presence of the mullite particles (Fig. 5) decreased, which is in agreement with the increase of the liquid phase viscosity (Fig. 4). The greatest decrease of foaming capacity was for the lowest BSA amount (5 vol%) and was similar for 10 and 15 vol% of BSA. As with BSA foams, the foaming capacity for aqueous mullite-BSA (10 and 15 vol%) suspensions was similar, with both significantly higher than the suspension with 5 vol%. However, if the variation of the Overrun % as a function of the stand time is taking into account, the presence of mullite particles did not substantially change its global behavior with time, which would indicate that the ceramic particles did not promote the stabilization of the foam. Fig. 5 shows that the Overrun % remained constant during the first 10–15 min and then slightly decayed to become nearly invariable after 20 min.

Contrary to that determined from Overrun %, the analysis of the remaining evaluated parameters revealed that the ceramic particles changed the properties of the BSA foams and also improved their stability. In Fig. 6b, it can be observed that the initial mullite-BSA foam wetness value (ϕ_{FW} at $t_R=0$) calculated from electric conductivity measurements increased

as a function of the BSA concentration (0.3–0.5), but these values were only slightly higher than those measured in foamed protein solutions with the same concentration. Thus, the foam wetness values obtained indicated that initially these foams were also wet foams. In the same way as in BSA foams, the foam wetness decreased by increasing the stand time, although this diminution occurred more slowly when mullite particles were present. Moreover, in all the range of analyzed time, the mullite-BSA foams were wetter than the corresponding protein foams. At 30 min, the mullite-BSA foams presented liquid fraction values about 0.2, higher than the foams produced from BSA solutions. Also, foamed mullite-BSA systems showed higher values of *FDS* % and a slower fall of this parameter with the stand time than BSA foams (Fig. 7), although the protein amount did not produce a significant effect on this parameter. Values of *FDS* % greater than 50% were registered at $t_R = 10$ min for all the BSA amounts. After 30 min, in all the mullite-BSA systems, *FDS* % was higher than 30%. In addition, the values of the time to half collapse ($t_{1/2}$) (Table 2) were significantly higher (11–13 min) than those obtained in BSA foams, although, these values remained rather independent of the BSA concentration. The bubbles immersed in the mullite suspension maintained the structural integrity for a longer stand time as this effect is less dependent on the protein concentration than in the case of the BSA solution. In particular, this fact can be associated with a higher viscosity of the liquid phase which can slow down the drainage rate due to a slower flowing of liquid through the foam network [15].

On the other hand, the mullite-BSA foams in general presented similar mean bubble sizes as a function of time, independent of the BSA concentration (Fig. 8 and Table 3). In all the mullite-BSA foams, lower mean bubble sizes and more uniform (lower *W*) bubble size distributions than the corresponding BSA foams were determined. This difference was more significant for the highest BSA concentration, which is in agreement with the fact that this suspension achieved the highest viscosity value. Moreover, for each BSA amount, the mean bubble size and width of bubble size distribution increased by increasing time, although this increment was not as pronounced as in the case of BSA foams. In spite of a smaller initial bubble size that can contribute to longer foam drainage [15], the obtained results can be attributed to the increase of the liquid phase viscosity produced by adding solid particles. In addition, the decrease of the evaluated parameters after the first 10 min together with the analysis of bubble size distributions as a function of the time can be mainly associated, as occurred in BSA foams, with the coarsening and coalescence processes, which more slowly operated than in the foamed protean system. Furthermore, in mullite-BSA foams, the occurrence of these processes together with the drainage of the liquid phase cannot be ruled out.

4. Conclusions

The studies carried out on the chemical and physical properties of aqueous mullite-albumin suspensions and foaming performance of this system are of great use for processing cellular ceramic materials by direct consolidation.

From the analysis of the colloidal stability of non-foamed aqueous mullite-BSA suspensions, it was assumed that the mullite suspension is suitably stabilized through synergistic interaction of the protein and the dispersant by electrosteric stabilization, in which a two-step adsorption of protein chains onto mullite particles occur. On the other hand, the apparent viscosity of the aqueous mullite suspension notably increased throughout the entire shear rate range by increasing the protein amount, with this increment much more marked at lowest shear rates. In addition, the dilatancy observed in the mullite suspension was decreasing, and the thixotropic thickening was significantly increasing by increasing the albumin content, which was associated with the rearrangement of the ceramic particles in the flow direction and extension of the protein chains, which could favor the formation of new and more stable structures.

The presence of ceramic particles in the protein foams decreased the foaming capacity and increased the stability of these foams. The bubbles immersed in the mullite suspension maintained this structural integrity for a longer stand time due to the higher viscosity of the liquid phase produced by adding solid particles that can slow down drainage rate. For both BSA foams and mullite-BSA foams, an increase in the protein content produced an increase in the foaming capacity. In all the range of analyzed time, the foam wetness and FDS % values of mullite-BSA foams were higher than the corresponding protein foams, and its decrease as a function of time occurred more slowly. In general, when mullite particles were present, the influence of the protein amount on foam properties was not so significant. Lower mean bubble sizes and more uniform bubble size distributions than the corresponding BSA foams were generated in all the mullite-BSA foams. The increase of both parameters by increasing time was lower than in the case of BSA foams.

Based on the results obtained, it was assumed that the foams destabilization occurred mainly by drainage during the first minutes of stand time, and before 10 min, the destabilization was attributed to coalescence and Ostwald ripening events, although the simultaneous occurrence of these processes cannot be ruled out. The presence of mullite particles significantly decreased the rate of these processes.

Acknowledgements

The authors gratefully acknowledge Dr. R. Moreno (Instituto de Cerámica y Vidrio, CSIC, Madrid, España) for carrying out the measurements of zeta potential. This study was supported by CONICET (Argentina) under project (PIP 0936, 2010-2012).

References

[1] S. Dhara, P. Bhargava, A simple direct casting route to ceramic foams, Journal of the American Ceramic Society 89 (10) (2003) 1645–1650.

[2] J. Luyten, S. Mullens, J. Cooymans, A.M. de Wilde, I. Thijs, R. Kemps, Differents methods to synthesize ceramics foams, Journal of the European Ceramic Society 29 (2009) 829–832.
[3] M. Scheffler, P. Colombo (Eds.), Cellular Ceramics: Structure, Manufacturing, Properties and Applications, Wiley—VCH, Weinheim, 2005.
[4] A.R.S. Studart, U.T. Gonzenbach, E. Tervoort, L.J. Gauckler, Processing routes to macroporous ceramics: a review, Journal of the American Ceramic Society 89 (2006) 1771–1789.
[5] H. Schneider, J. Schreuer, B. Hildmann, Structure and properties of mullite—a review, Journal of the European Ceramic Society 28 (2) (2008) 329–344.
[6] M.I. Osendi, C. Baudín, Mechanical properties of mullite materials, Journal of the European Ceramic Society 16 (2) (1996) 217–224.
[7] F. Orgaz, Densification and crystallization kinetics of mullite diphasic gels from non_isothermal dilatometric experiments, Boletín de la Sociedad Española de Cerámica y Vidrio 47 (2008) 358–365.
[8] U.T. Gonzenbach, A.R. Studart, D. Steinlin, E. Tervoort, L.J. Gauckler, Macroporous ceramics from particle-stabilized wet foams, Journal of the American Ceramic Society 90 (2007) 16–22.
[9] O. Lyckfeldt, J. Brandt, S. Lesca, Protein forming—a novel shaping technique for ceramics, Journal of the European Ceramic Society 20 (2000) 2551–2559.
[10] I. Garrn, C. Reetz, N. Brandes, L.W. Kroh, H. Schubert, Clot-forming: the use of proteins as binders for producing ceramic foams, Journal of the European Ceramic Society 24 (2004) 579–587.
[11] S. Bhattacharjee, L. Besra, B.P. Singh, Effect of additives on the microstructure of porous alumina, Journal of the European Ceramic Society 27 (2007) 47–52.
[12] L.A. Glaser, A.T. Paulson, R.A. Speers, R.Y. Yada, D. Rousseau, Foaming behavior of mixed bovine serum albumin-protamime systems, Food Hydrocolloids 21 (2007) 495–506.
[13] S. Damodaran, Protein stabilization of emulsions and foams, Journal of Food Science 70 (3) (2005) 54–66.
[14] E.A. Foegeding, P.J. Luck, J.P. Davis, Factors determining the physical properties of protein foams, Food Hydrocolloids 20 (2–3) (2006) 284–292.
[15] X. Yang, E.A. Foegeding, The stability and physical properties of egg white and whey protein foams explained based on microstructure and interfacial properties, Food Hydrocolloids 25 (2011) 1687–1701.
[16] A. Fadli, I. Sopyan, Porous ceramics with controllable properties prepared by protein foaming-consolidation method, Journal of Porous Materials 18 (2011) 195–203.
[17] S. Dhara, Influence of slurry characteristics on porosity and mechanical properties of alumina foams, International Journal of Applied Ceramic Technology 3 (5) (2006) 382–392.
[18] M.A. Camerucci, Desarrollo y evaluación de materiales cerámicos de cordierita y cordierita-mullita, Ph.D. National University of Mar del Plata, Argentina, 1999.
[19] R. Wojciechowska, W. Wojciechowski, J. Kaminski, Thermal decompositions of ammonium and potassium alums, Journal of Thermal Analysis 33 (1988) 503–509.
[20] K. Murayama, M. Tomida, Heat induced secondary structure and conformation change of bovine serum albumin investigated by Fourier transform infrared spectroscopy, Biochemistry 43 (2004) 11526–11532.
[21] S. Damodaran, A. Paraf (Eds.), Food Proteins and their Applications, Marcel Dekker, New York, 1997.
[22] K. Rezwan, L.P. Meier, M. Rezwan, J. Vörös, M. Textor, L.J. Gauckler, Bovine serum albumin adsorption onto colloidal Al_2O_3. Particles: a new model based on zeta potential and UV–vis measurements, Langmuir 20 (2004) 10055–10061.
[23] M.H. Talou, M.A. Villar, M.A. Camerucci, R. Moreno, Rheology of aqueous mullite-starch suspensions, Journal of the European Ceramic Society 31 (2011) 1563–1571.
[24] F.S. Ortega, Produção e caracterização de espumas cerámicas obtidas pelo proceso gelcasting, Ph.D. Doutorado em Ciência e Engenharia de Materiais, Universidade Federal de São Carlos, São Carlos, 2002.
[25] A. Kato, A. Takahashi, N. Matsudomi, K. Kobayashi, Determination of foaming properties of proteins by conductivity measurements, Journal of Food Science 48 (1983) 62–65.
[26] M. Barigou, N.S. Deshpande, F.N. Wiggers, An enhanced electrical resistance technique for foam drainage measurement, Colloids and Surfaces A: Physicochemical and Engineering Aspects 189 (2001) 237–246.
[27] A. Phianmongkhol, J. Varley, A multi point conductivity measurement system for characterisation of protein foams, Colloids and Surfaces B: Biointerfaces 12 (1999) 247–259.
[28] D.J. Wright, J.W. Hemmant, Foaming properties of protein solutions: comparison of large-scale whipping and conductimetric methods, Journal of the Science of Food and Agriculture 41 (1987) 361–371.
[29] P.J. Luck, N. Bray, E.A. Foegeding, Factors determining yield stress and Overrun of whey protein foams, Journal of Food Science 67 (2001) 1677–1681.
[30] A. Raymundo, J. Empis, I. Sousa, Method to evaluate foaming performance, Journal of Food Engineering 36 (1998) 445–452.
[31] Y. Liang, H.G. Kristinsson, Influence of pH-induced unfolding and refolding of egg albumen on its foaming properties, Journal of Food Science 70 (2005) C222–C230.
[32] L. Indrawati, G. Narsimhan, Characterization of protein stabilized foam formed in a continous shear mixing apparatus, Journal of Food Engineering 88 (2008) (465–465).
[33] T.D. Karapantsios, M. Papara, On the design of electrical conductance probes for foam drainage applications Assesment of ring electrodes performance and bubble size effects on measurements, Colloids and Surfaces A: Physicochemical and Engineering Aspects 323 (2008) 139–148.
[34] A. Krajewski, A. Piancastelli, R. Malavolti, Albumin adhesion on ceramics and correlation with their Z-potential, Biomaterials 19 (1998) 637–641.
[35] M.H. Talou, Procesamiento de materiales cerámicos porosos de mullita por consolidación directa con almidón, Thesis Doctoral, Universidad Nacional de Mar del Plata, 2012.
[36] R. Moreno, Reología de suspensiones cerámicas. Consejo Superior de Investigaciones Científicas, Madrid, Spain, 2005.
[37] B.S. Murray, Stabilization of bubbles and foams, Current Opinion in Colloid and Interface Science 12 (2007) 232–241.
[38] J.R. Clarkson, Z.F. Cui, R.C. Darton, Protein denaturation in foam I. Mechanism study, Journal of Colloid and Interface Science 215 (1999) 323–332.